Geophysica (1995), 31, 1-21

Numerical Modeling for the Effect of a 2-D Seafloor Trench on Sea-Bottom EM Measurements Using Horizontal Electric Dipole Sources

G. Pethő[1], *P. Kaikkonen*[2] *and L.L. Vanyan*[3]

[1] University of Miskolc, Dept. of Geophysics, H-3515 Miskolc, Hungary
[2] University of Oulu, Dept. of Geophysics, FIN-90570 Oulu, Finland
[3] P.P. Shirshov Institute of Oceanology, 117218 Moscow, Krasikova, 23, Russia

(Received: August 1994; Accepted: January 1995)

Abstract

The paper presents the comparison of the frequency domain EM responses of a two-dimensional (2-D) seafloor trench to a horizontal electric dipole source to be parallel and perpendicular to the strike. The EM field components are computed along an in-line horizontal seafloor profile perpendicular to the axis of the trench at two frequencies. The chosen numerical procedure is a finite-difference method after a Fourier transform of Maxwell's equations from the space domain (x,y,z) to the along-strike wavenumber domain (k_x,y,z). In this way the original three-dimensional (3-D) problem is derived to a set of 2-D ones. The spatial electromagnetic field components are then determined numerically by an inverse Fourier transform. If the horizontal electric source situated at the seafloor is perpendicular to the structural strike direction, the EM responses computed over the trench are sharper than those due to electric source parallel to the strike. The seafloor topographic effect on EM frequency sounding responses must be taken into account in order to avoid misinterpretation.

Key words: marine geophysics, controlled-source electromagnetics, electromagnetic modelling

1. *Introduction*

Marine controlled-source electromagnetic systems for the exploration of seafloor operate in both frequency and time domain. *Chave* and *Cox* (1982) developed the theory of the frequency domain method using horizontal and vertical electric dipole sources and derived closed-form expressions for the electromagnetic induction fields in the conducting ocean overlying a one-dimensional earth. *Edwards* and *Chave* (1986) determined the transient responses of two conductive, adjoining half-spaces to an electric dipole-dipole system located on the seafloor. As the more interesting areas of the seafloor are clearly not 1-D, the increasing interest in marine controlled-source systems led *Everett* and *Edwards* (1993) to solve the 2.5-D forward problem of transient marine electromagnetics. Finite-element method was used to solve the frequency domain electromagnetic response of a 2-D earth under the excitation of a 3-D current source by *Unsworth, Travis* and *Chave* (1993) as well. The ever increasing computer facilities and developments in finite-difference and finite-

element methodology make it possible to determine the effect of 2-D seafloor topography on marine controlled-source electromagnetic field components.

In this paper a finite-difference method is presented to demonstrate the effect of an elongated rectangular seafloor trench on EM components. *Stoyer* and *Greenfield* (1976) developed a finite-difference formulation to determine the response of a 2-D conductivity structure to an oscillating magnetic dipole source. Their formulation is general, and the EM response of a 2-D earth under the excitation of electric dipole source can be modeled as well. This kind of modeling using horizontal electric dipole sources was carried out by *Pethő* and *Kaikkonen* (1993) making a comparison between frequency sounding response of a 2-D step-like structure to an electric dipole source parallel and perpendicular to the geological strike. As it was expected the EM responses computed for the in-line array with a transmitter perpendicular to the strike were more sensitive to the model than those to an along-strike electric dipole source. In the course of seafloor EM survey the topographical changes of the seafloor can have influence on the EM components. These topographical inhomogeneities are 3-D ones. However, they are frequently elongated in one direction and can be treated as 2-D seamounts or 2-D trenches. The goals of this model study are to present this method for frequency domain marine controlled-source electromagnetic measurements using horizontal electric dipole sources, and to illustrate how the EM responses are affected by a 2-D trench.

2. *Mathematical formulation*

The basic relationships governing this electromagnetic phenomenon are Maxwell's equations. Assuming e^{jwt} time dependent electric source they are:

$$rot\,\vec{E} = -j\omega\mu\vec{H} \tag{1}$$

$$rot\,\vec{H} = (\sigma + j\omega\varepsilon)\vec{E} + \vec{i_s};\ \vec{i_s} = I\,d\vec{s}\,\delta\ (\vec{r}) \tag{2}$$

where $\vec{i_s}$ is the current density. If equations (1), (2) are reduced to components in the x,y,z directions then the Fourier transforms of the equations can be determined over the strike direction (x). If G denotes any component of $\vec{E}$ or $\vec{H}$, the Fourier transform of G over x is:

$$\tilde{G}(k_x,y,z) = \int_{-\infty}^{\infty} G(x,y,z)\, e^{-jk_x x}\,dx \tag{3}$$

Throughout the paper a tilde is used to denote quantities in the Fourier transform domain. The Fourier transform of the function $\dfrac{\partial G}{\partial x}$ over x is $(-jk_x)$ times $\tilde{G}(k_x,y,z)$ because $G(x,y,z)$

vanishes as $x \to \pm\infty$. Taking into consideration the relationships above and assuming only an electric source parallel to the strike the densest form of the Fourier transform of the component equations (1), (2) is the following partial differential equations:

$$-\frac{\partial}{\partial y}\left(\frac{1}{\zeta^M}\frac{\partial \tilde{H}_x}{\partial y}\right)-\frac{\partial}{\partial z}\left(\frac{1}{\zeta^M}\frac{\partial \tilde{H}_x}{\partial z}\right)-jk_x\frac{\partial \xi}{\partial y}\frac{\partial \tilde{E}_x}{\partial z}+jk_x\frac{\partial \xi}{\partial z}\frac{\partial \tilde{E}_x}{\partial y}+\Upsilon^M\tilde{H}_x=0 \tag{4}$$

$$-\frac{\partial}{\partial y}\left(\frac{1}{\zeta^E}\frac{\partial \tilde{E}_x}{\partial y}\right)-\frac{\partial}{\partial z}\left(\frac{1}{\zeta^E}\frac{\partial \tilde{E}_x}{\partial z}\right)+jk_x\frac{\partial \xi}{\partial y}\frac{\partial \tilde{H}_x}{\partial z}-jk_x\frac{\partial \xi}{\partial z}\frac{\partial \tilde{H}_x}{\partial y}+\Upsilon^E\tilde{E}_x=-\tilde{i}_{sx} \tag{5}$$

(4), (5) are called the Transverse Magnetic (TM) and the Transverse Electric (TE) equation, respectively. In these equations $\tilde{H}_x$, $\tilde{E}_x$ are the Fourier transforms of H_x and E_x over x; $\tilde{i}_{sx}$ is the Fourier transform of the electric source term in the strike direction. If k denotes the wavenumber, ξ, TM admittance, TE impedance, TE admittance, TM impedance can be defined after *Stoyer and Greenfield* (1976) in the following way: $k^2 = \omega^2 \mu \varepsilon - j\omega\mu\sigma$; $\xi = (k_x^2 - k^2)^{-1}$; $\Upsilon^M = j\omega\mu$; $\zeta^E = (1-k_x^2/k^2)\Upsilon^M$; $\Upsilon^E = (\sigma + j\omega\varepsilon)$; $\zeta^M = (1-k_x^2/k^2\Upsilon^E$.

In comparison with (4), (5) there are differences only in the right-hand sides of these equations if the source is parallel to the y direction (i.e. perpendicular to the geological strike):

$$-\frac{\partial}{\partial y}\left(\frac{1}{\zeta^M}\frac{\partial \tilde{H}_x}{\partial y}\right)-\frac{\partial}{\partial z}\left(\frac{1}{\zeta^M}\frac{\partial \tilde{H}_x}{\partial z}\right)-jk_x\frac{\partial \xi}{\partial y}\frac{\partial \tilde{E}_x}{\partial z}+jk_x\frac{\partial \xi}{\partial z}\frac{\partial \tilde{E}_x}{\partial y}+\Upsilon^M\tilde{H}_x= \tag{6}$$

$$=-\frac{\partial}{\partial z}\left(\frac{\tilde{i}_{sy}}{\zeta^M}\right)$$

$$-\frac{\partial}{\partial y}\left(\frac{1}{\zeta^E}\frac{\partial \tilde{E}_x}{\partial y}\right)-\frac{\partial}{\partial z}\left(\frac{1}{\zeta^E}\frac{\partial \tilde{E}_x}{\partial z}\right)+jk_x\frac{\partial \xi}{\partial y}\frac{\partial \tilde{H}_x}{\partial z}-jk_x\frac{\partial \xi}{\partial z}\frac{\partial \tilde{H}_x}{\partial y}+\Upsilon^E\tilde{E}_x= \tag{7}$$

$$=jk_x\frac{\partial}{\partial y}(\xi\tilde{i}_{sy})$$

In order to model 2-D inhomogeneities the structures and their surroundings are covered with a finite rectangular grid. The distributed parameters of equations (4)-(7) are constant within each rectangular grid element and any part of the geologic cross section with distributed parameters can be replaced by a grid section consisting of lumped circuit elements as it is shown in Figure 1. Using the transmission sheet analogy according to *Stoyer* and *Greenfield* (1976) the finite difference forms of the partial differential equations (4), (5) or (6), (7) are:

$$\sum_{i=1}^{4}\left[\frac{\tilde{H}_{ix}-\tilde{H}_{ox}}{-Z_i^M}+\frac{\tilde{E}_{ix}-\tilde{E}_{ox}}{C_i}\right]+Y_o^M\tilde{H}_{ox}=\tilde{S}_o^M \tag{8}$$

$$\sum_{i=1}^{4}\left[\frac{\tilde{E}_{ix}-\tilde{E}_{ox}}{-Z_i^E}+\frac{\tilde{H}_{ix}-\tilde{H}_{ox}}{C_i}\right]+Y_o^E\tilde{E}_{ox}=\tilde{S}_o^E \tag{9}$$

where Z denotes lumped impedances, C denotes coupling terms between the central and one of the four neighbouring nodes, Y represents lumped admittances and S stands for source terms.

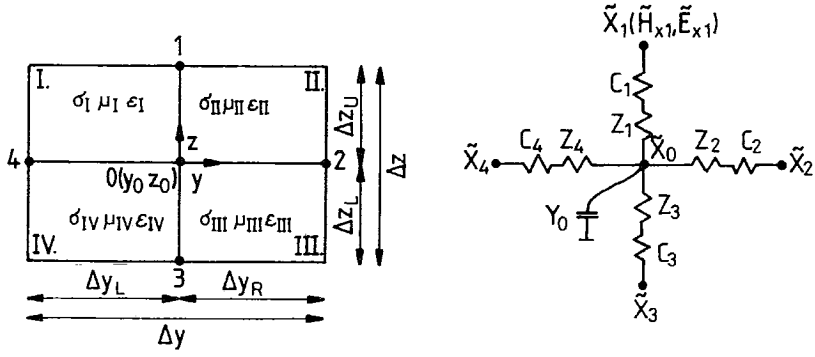

Fig. 1. Grid section of the 2-D model and its electric circuit analogy in the (k_x,y,z) domain.

The reciprocal values of coupling terms - which do not occur in magnetotellurics - are directly proportional to values ξ of the adjacent elements and are independent of the size of elements. For example Z_I^M, C_I and Y_o^M can be given by the formulae:

$$\frac{1}{Z_1^M}=\frac{2}{\Delta z_U}\left(\frac{\Delta y_R}{\zeta_{II}^M}+\frac{\Delta y_L}{\zeta_I^M}\right) \tag{10}$$

$$\frac{1}{C_1}=2jk_x\left(\xi_I-\xi_{II}\right) \tag{11}$$

$$Y_o^M=\Delta y_L\Delta z_U\Upsilon_I^M+\Delta y_R\Delta z_U\Upsilon_{II}^M+\Delta y_R\Delta z_L\Upsilon_{III}^M+\Delta y_L\Delta z_L\Upsilon_{IV}^M \tag{12}$$

The coupled partial differential equations (4), (5) or (6), (7) are very similar to those of two coupled transmission sheets and this analogy makes it possible to fulfil the interior boundary conditions, because each gridpoint can be considered as a branch point of circuit. Along the edge of the grid terminal-impedance type boundary condition was used, i.e. the edge of the mesh was grounded. Instead of the plane-wave, terminal-impedance type bound-

ary condition the fraction of the inward-directed lumped impedance was taken as the outward-directed lumped impedance at all edges of the grid.

The electric sources are treated in the way as the magnetic sources were considered by *Stoyer* (1974) and *Takács* (1979). They are assumed to have no extension in the structural strike direction, and constant σ, μ, ε values are supposed in their vicinity.

The electric source in the strike direction (in equation (5)) is treated like a distributed parameter in four quarter grid elements surrounding the node where the source is applied. The lumped source term (in equation (9)) is the average value over the area being lumped. The electric source perpendicular to the strike (in equations (6), (7)) is treated as Heaviside function of space in the x=0 plane as well: it is smeared within a rectangular grid element so as to take its derivatives with respect to y and z. The derivatives of step function are taken across element boundaries along the line segments connecting the mid-points of neighbouring grid elements. They can be expressed in the terms of weighted delta functions. These derivatives are lumped over the line segments and then referred to the neighbouring two nodes on the element boundary. In this way there is only one grid node with a source term different from zero if the electric source is parallel to the strike direction, and there are four nodes which yield inhomogeneous finite-difference TM and TE equations if the applied electric source is perpendicular to the structural strike.

During the solution of the linear set of equations the block tridiagonal structure of the coefficient matrix was taken into account, and the order of the greatest real matrix to be inversed was 4Mx4M where M denotes the number of rows. The applied method was the LU decomposition for which details were given by *Pethő* (1987).

In order to get the EM responses in the space domain the solutions of the wavenumber domain have to be inverse Fourier transformed. For source free area and for the plane which is perpendicular to the strike and contains the source this transformation becomes simple. If $\tilde{L}$ denotes the Fourier transform of the in-phase or out-of-phase components of the along-strike EM fields ($\tilde{E}_x IP$, $\tilde{E}_x Q$, $\tilde{H}_x IP$, $\tilde{H}_x Q$) and $\tilde{L}_i$ denotes their partial derivatives with respect to y or z, the spatial in-phase and out-of-phase components of the along-strike EM fields can be calculated on the basis of (13) and, on the other hand, the in-phase and out-of-phase components of the off-strike EM fields can be determined according to (14):

$$L(0,y,z) = \frac{1}{\pi} \int_{k_x=0}^{k_x\max} \tilde{L}(k_x,y,z)\,dk_x \tag{13}$$

$$G(0,y,z) = \frac{1}{\pi} \int_{k_x=0}^{k_x\max} \left[\frac{c_1 \tilde{L}_1(k_x,y,z)}{k_x^4 + a^4} + \frac{c_2 k_x \tilde{L}_2(k_x,y,z)}{k_x^4 + a^4} + \frac{c_3 k_x^2 \tilde{L}_3(k_x,y,z)}{k_x^4 + a^4} + \frac{c_4 k_x^3 \tilde{L}_4(k_x,y,z)}{k_x^4 + a^4} \right] dk_x \tag{14}$$

In equation (14) $a = \sqrt{\omega\,\mu\,\sigma}$

For electric sources parallel to the structural strike the EM components different from zero in the plane x=0 can be calculated with (13), (14) through Table 1.

Table 1. Expressions used in (13) and (14) to determine the in-phase (*IP*) and out-of-phase (*Q*) EM components in the plane containing the electric source parallel to the strike.

L $\quad$ $\tilde{L}$
E_xIP $\quad$ $\tilde{E}_xIP$
E_xQ $\quad$ $\tilde{E}_xQ$

G	c_1	$\tilde{L}_1$	c_2	$\tilde{L}_2$	c_3	$\tilde{L}_3$	c_4	$\tilde{L}_4$
H_yIP	$-\omega\mu\sigma^2$	$\frac{\partial \tilde{E}_xQ}{\partial z}$	$-\omega\mu\sigma$	$\frac{\partial \tilde{H}_xIP}{\partial y}$	$-\sigma$	$\frac{\partial \tilde{E}_xIP}{\partial z}$	1	$\frac{\partial \tilde{H}_xQ}{\partial y}$
H_yQ	$-\omega\mu\sigma^2$	$\frac{\partial \tilde{E}_xIP}{\partial z}$	$-\omega\mu\sigma$	$\frac{\partial \tilde{H}_xQ}{\partial y}$	$-\sigma$	$\frac{\partial \tilde{E}_xQ}{\partial z}$	-1	$\frac{\partial \tilde{H}_xIP}{\partial y}$
H_zIP	$-\omega\mu\sigma^2$	$\frac{\partial \tilde{E}_xQ}{\partial y}$	$-\omega\mu\sigma$	$\frac{\partial \tilde{H}_xIP}{\partial z}$	σ	$\frac{\partial \tilde{E}_xIP}{\partial y}$	1	$\frac{\partial \tilde{H}_xQ}{\partial z}$
H_zQ	$-\omega\mu\sigma^2$	$\frac{\partial \tilde{E}_xIP}{\partial y}$	$-\omega\mu\sigma$	$\frac{\partial \tilde{H}_xQ}{\partial z}$	σ	$\frac{\partial \tilde{E}_xQ}{\partial y}$	-1	$\frac{\partial \tilde{H}_xIP}{\partial z}$

In the second case when the horizontal electric dipole source is perpendicular to the structural strike the EM components of the in-line arrangement can be determined by means of equations (13), (14) and Table 2.

Table 2. Expressions used in (13) and (14) to determine the in-phase (*IP*) and out-of-phase (*Q*) EM components in the plane containing the electric source perpendicular to the strike.

L $\quad$ $\tilde{L}$
H_xIP $\quad$ $\tilde{H}_xIP$
H_xQ $\quad$ $\tilde{H}_xQ$

G	c_1	$\tilde{L}_1$	c_2	$\tilde{L}_2$	c_3	$\tilde{L}_3$	c_4	$\tilde{L}_4$
E_yIP	$-\omega\mu^2\mu^2\sigma$	$\frac{\partial \tilde{H}_xIP}{\partial z}$	$-\omega\mu\sigma$	$\frac{\partial \tilde{E}_xIP}{\partial y}$	$-\omega\mu$	$\frac{\partial \tilde{H}_xQ}{\partial z}$	1	$\frac{\partial \tilde{E}_xQ}{\partial y}$
E_yQ	$-\omega\mu^2\mu^2\sigma$	$\frac{\partial \tilde{H}_xQ}{\partial z}$	$-\omega\mu\sigma$	$\frac{\partial \tilde{E}_xQ}{\partial y}$	$\omega\mu$	$\frac{\partial \tilde{H}_xIP}{\partial z}$	-1	$\frac{\partial \tilde{E}_xIP}{\partial y}$
E_zIP	$-\omega^2\mu^2\sigma$	$\frac{\partial \tilde{H}_xIP}{\partial y}$	$-\omega\mu\sigma$	$\frac{\partial \tilde{E}_xIP}{\partial z}$	$\omega\mu$	$\frac{\partial \tilde{H}_xQ}{\partial y}$	1	$\frac{\partial \tilde{E}_xQ}{\partial z}$
E_zQ	$-\omega^2\mu^2\sigma$	$\frac{\partial \tilde{H}_xQ}{\partial y}$	$-\omega\mu\sigma$	$\frac{\partial \tilde{E}_xQ}{\partial z}$	$-\omega\mu$	$\frac{\partial \tilde{H}_xIP}{\partial y}$	-1	$\frac{\partial \tilde{E}_xIP}{\partial z}$

The spatial electromagnetic field components are determined numerically. Choosing logarithmically equidistant sampling in the spatial wavenumber domain, each $\tilde{L}$ and $\tilde{L}_i$ function is approximated by a second-order polynomial function for each section of k_x, where one section is determined by three discrete k_x values, and the third k_x value of each section is the first k_x value of the next one. Owing to the abrupt decrease of each function

of $\tilde{L}$ and $\tilde{L}_i$ with increasing k_x it was sufficient to evaluate the integrals (13), (14) to a certain value of k_x.

3. *Numerical results and discussion*

In this part the results of the 2-D modeling are presented. Before modeling both the grid (its horizontal and its vertical spacings and its extension as well) and the along-strike wavenumbers (the range and the distribution of the discrete wavenumbers) have to be planned. The applied planning procedure is usually as follows: the EM responses of different horizontally stratified half-spaces corresponding to the different 1-D parts of the 2-D section to be modeled are determined by 1-D forward modeling on the basis of linear filtering developed by *Anderson* (1979) and by the 2-D program. The 1-D forward modeling results are considered as reference results. *Pethő* and *Kaikkonen* (1993) found that grid spacing requirements for the largest frequency suggested by *Stoyer* and *Greenfield* (1976), a larger extension of the grid (due to the frequencies), and the wavenumber values of k_{x1}=0 m^{-1} and k_{xi}=2.10^{-5}.1,5$^{(i-2)}$ m^{-1} where i=2,3,...,15 resulted in an acceptable agreement between the reference values of 1-D program and the results of 2-D program over a two-layer half-space using transmitter-receiver range of 8 km≤R≤16 km at the frequency range of 0,1 Hz≤f≤4 Hz. This test of accuracy was only made for the electric field components parallel to the source direction. The better agreement was attained to the electric field components of the dipole equatorial array: it was within 2 percent in amplitude and 1 degree in phase. Although a finer grid (49 columns x 35 rows as compared with 46x30) was used to determine the electric field of the two-layer half-space to a dipole axial array, it did not manage to attain the accuracy of the first case. In contrast to (13) the electric field of the dipole axial array (E_y) is determined by (14) and its accuracy was 4 percent in amplitude and 8 degrees in phase. Comparing normalized amplitude and normalized phase responses of different 1-D models at the same transmitter-receiver array calculated by 1-D and 2-D numerical modeling, it was experienced that the accuracy of the 2-D numerical modeling increased due to the normalization. To get accurate solution for all EM components requires even more consideration. Figure 2 and Figure 3 show the comparison of EM responses of a two-layer half-space to a dipole equatorial and to an axial array computed by 1-D and 2-D program at the frequency of f=0,666 Hz. The thickness of the first layer was 2000 m, and the resistivities were ρ_1=10 Ωm and ρ_2=100 Ωm. The inverse transformations for all EM components were carried out for the same 15 along-strike wavenumbers as mentioned above and the same grid with 141x28 nodes was used for the two source polarizations. If the range of wavenumber is increased, unstable solutions can develop for the off-strike EM components. At the same time, additional inverse numerical transformations over k_x are suggested to increase the accuracy of E_x and H_x. A finer sampling with respect to k_x and the use of smaller vertical grid elements resulting in greater number of rows can be suggested to enhance the accuracy of the off-strike components.

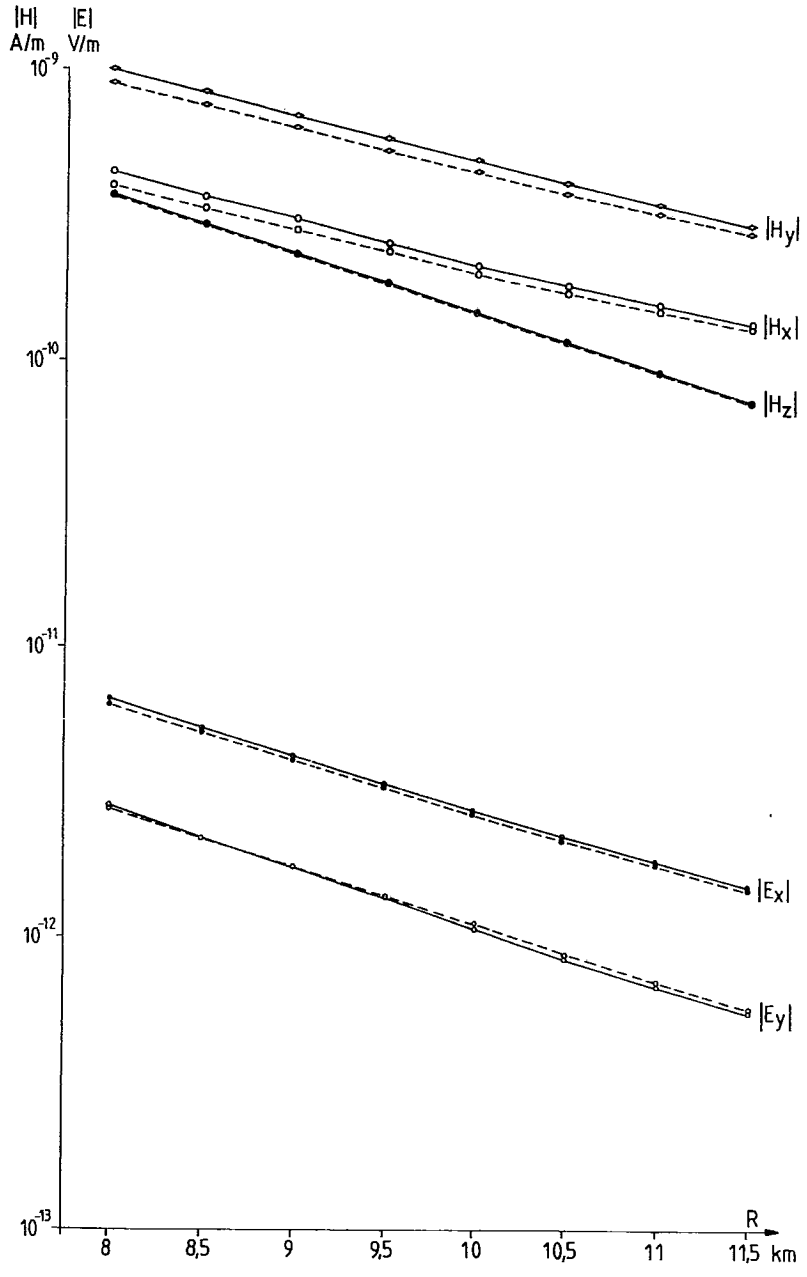

Fig. 2. Amplitude responses of a horizontally stratified two-layer half-space with ρ_1=10 Ωm, h_1=2000 m, ρ_2=100 Ωm to dipole equatorial (E_x, H_y, H_z) and to dipole axial array (E_y, H_x) at the frequency of f=0,666 Hz. The solid line is for the responses calculated by 1-D modeling, and the dashed line respresents amplitude responses determined by 2-D finite-difference modeling.

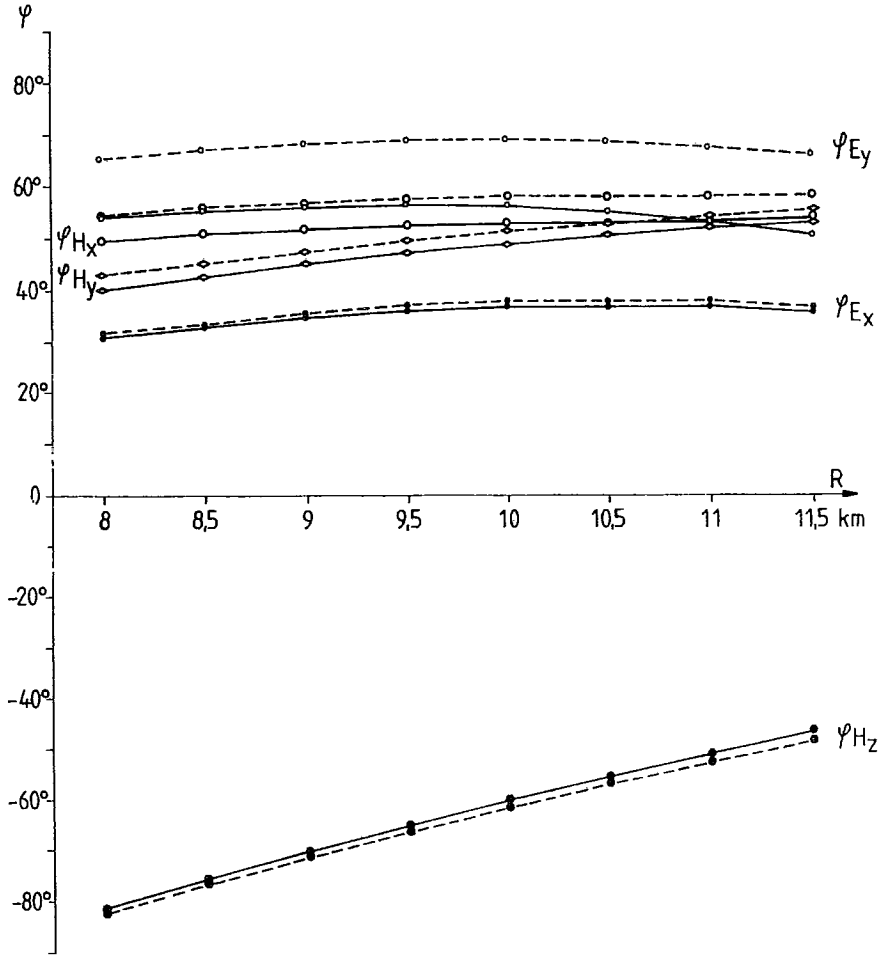

Fig. 3. Phase responses of a horizontally stratified two-layer half-space to dipole equatorial and to dipole axial array. Otherwise see Figure 2.

Figure 4 presents a 2-D analog and numerical modeling comparison over a step-like structure. The EM scale model measurements were planned and carried out by *Szarka* (1993), and the numerical modeling was done by the finite-difference method described

in this paper. In order to decrease the error of the off-strike electric field component a finer grid (49x35) was used to cover the step instead of the one (46x30) applied for the dipole equatorial array. The normalized amplitude frequency sounding curves of the electric field components to the two source polarizations are given. The reference model was the homogeneous two-layer half-space corresponding to the left-hand side of the step. The model is presented in Figure 4. In spite of the departures, the similar behaviour of the analog and numerical normalized amplitude frequency sounding curves of the electric

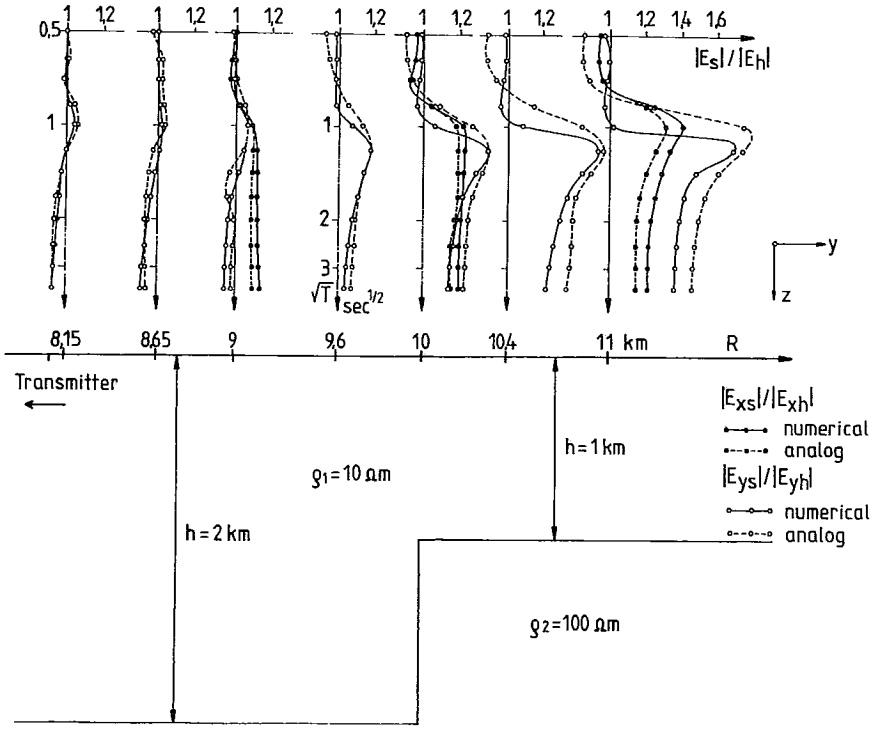

Fig. 4. Normalized amplitudes of horizontal electric field components over a step-like structure to an electric dipole source parallel (x) and perpendicular (y) to the structural strike as a function of time period and transmitter-receiver offset determined by analog and numerical modeling.

fields to the same array can be observed. If the electric field is perpendicular to the strike (dipole axial array) the responses are more sensitive to the structure. The reason for the departures may be the moderate resistivity contrast (1 to 10) of the structure, which is difficult to model in lab conditions. On the other hand, the off-strike electric field components determined numerically will contain considerably more error even after the normalization than the along-strike electric field components have.

In the course of marine controlled-source electromagnetic numerical modeling the EM fields to horizontal electric dipole (HED) sources were determined by similar transmitter-receiver distances as in the case of step model, and they were calculated at two frequencies within the frequency range of that modeling. Throughout the numerical modeling the current strength of the HED source was 1A independent of the array. The discrete wavenumbers were chosen as they were selected for the step model: after k_{x1}=0 m^{-1} they were taken as $k_{xi}=2.10^{-5}.1,4^{(i-2)}$ m^{-1} where i=2,3,...,15. In order to enhance the response of the 2-D seafloor structure normalized amplitudes (the ratio of the amplitude response of inhomogeneous model to that of homogeneous one) and relative phases (phase response difference between the inhomogeneous and homogeneous model) were taken at the same transmitter-receiver distances along the profile. This reference model was defined as a homogeneous horizontally stratified model with the sea water (ρ_4=0,3 Ωm, h_4=3 km), the upper layer of the crust ($\rho_1=10^3$ Ωm, h_1= 5 km) and the lower "infinite" one ($\rho_2=10^4$ Ωm). In this way the normalized responses calculated along the horizontal seafloor profile are free from the effect of transmitter-receiver offsets as well. The 2-D structure to be modeled is shown in the lower part of Figure 6. The inhomogeneity in the upper layer of the crust, the sea mount and the trench make a difference between the 2-D model and the horizontally stratified space described earlier. At the two frequencies two grids were used. The conductivity distribution, horizontal and vertical grid spacings are presented at the frequency of f=0,1 Hz in Figure 5. The 2-D seafloor trench is denoted by 5x3 digits of 4 in the right-hand side of the conductivity section map under the horizontal line separating the the sea water (digit 4) from the crust (digit 1) at the depth of 3 km. This coarse grid has 120 columns and 43 rows in contrast with the finer grid of 148 columns and 45 rows applied to f=1 Hz. Figure 6 shows how the amplitude of E_{yh} (subscript h denotes the homogeneous model) developes as a function of k_x in the case of the homogeneous model at the frequency of f=0,1 Hz. There is no great difference between the amplitudes of E_{yh} determined after the 13th and the 15th k_x values on the right-hand side of the profile at larger transmitter-receiver offsets. The left-hand side of the amplitude profile curve of E_{yh} after the 15th k_x value graphically coincides with the same part of $|E_{yi}|_{15}$ amplitude response of the inhomogeneous structure to the electric dipole source perpendicular to the strike. Similar responses were computed for the other source direction and at the other frequency for all along-strike and off-strike EM field responses without getting unstable solutions.

Horizontal spacings:
7000. 7000. 7000. 7000. 7000. 7000. 7000. 7000. 7000. 6500.
6500. 4500. 3500. 2500. 1700. 1300. 1000. 800. 700. 500.
500. 500. 500. 500. 500. 400. 400. 400. 300. 200.
200. 200. 200. 200. 300. 400. 400. 400. 400. 400.
400. 400. 400. 400. 400. 400. 400. 400. 400. 400.
400. 400. 400. 400. 400. 300. 300. 200. 200. 200.
200. 200. 200. 200. 200. 200. 200. 200. 200. 200.
200. 200. 200. 200. 200. 200. 200. 200. 200. 200.
200. 200. 200. 200. 200. 200. 200. 200. 200. 200.
200. 200. 200. 300. 300. 400. 400. 500. 500. 500.
500. 700. 800. 1000. 1200. 1500. 2000. 2500. 3500. 4800.
7000. 7000. 7000. 7000. 7000. 7000. 7000. 7000. 7000.
Vertical spacings:
800. 600. 500. 300. 200. 200. 200. 200. 200. 200.
200. 200. 300. 500. 800. 1300. 1300. 1300. 1900. 2900.
4200. 6300. 6400. 7000. 7000. 7000. 7000. 7000. 7000. 7000.
7000. 7000. 7000. 7000. 7000. 7000. 7000. 7000. 7000. 7000.
7000. 7000.

Conductivity map

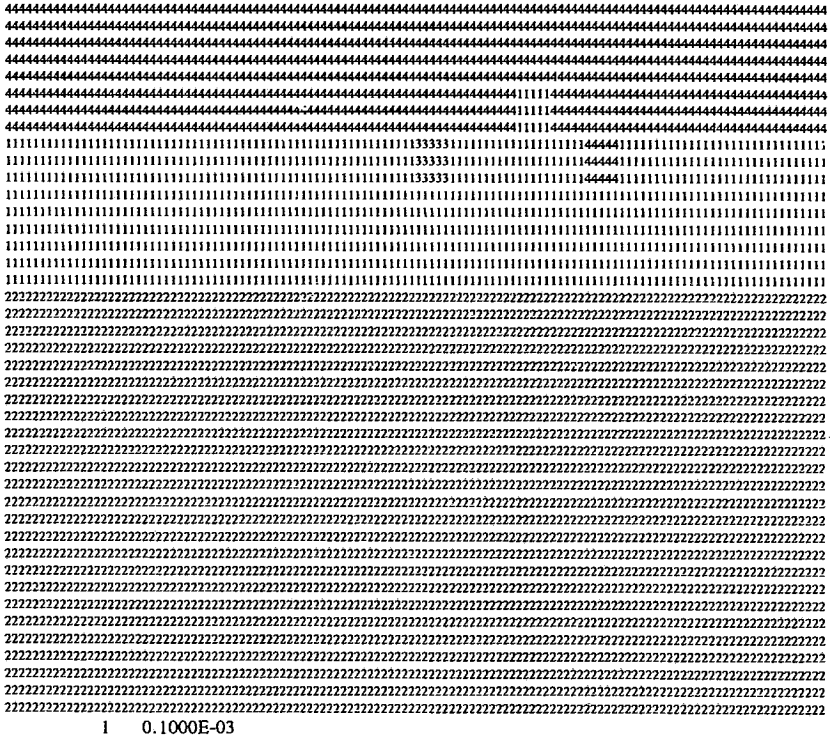

1 0.1000E-03
2 0.1000E-02
3 0.1000E-01
4 0.3330E+01

Source position column and row: 33, 9
Frequency: 0.1 Hz

Fig. 5. Input data characterizing the grid geometry and the conductivity distribution of the 2-D structure shown in the lower part of Figure 6 at the frequency of f=0,1 Hz.

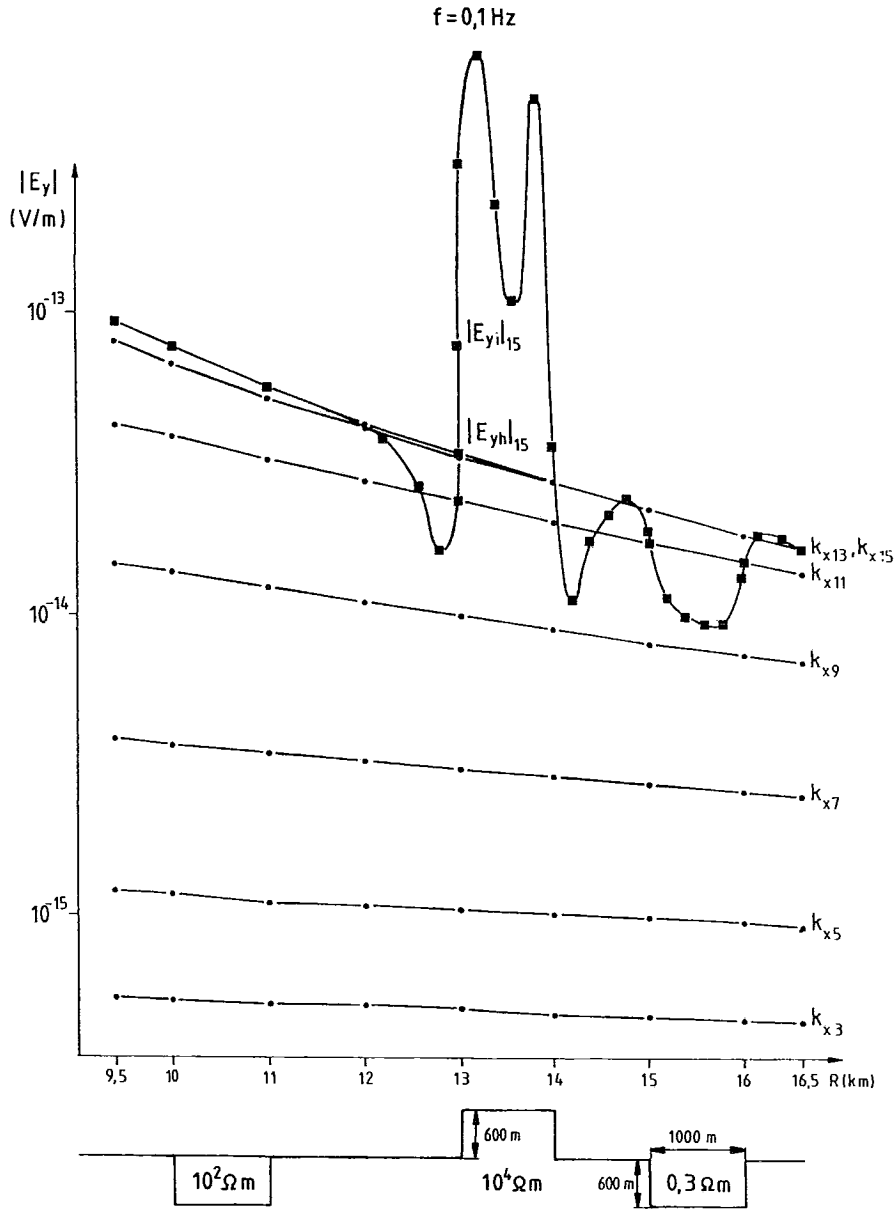

Fig. 6. $|E_y|$ components as a function of R, transmitter-receiver distance at different wavenumbers for homogeneous horizontally stratified structure and $|E_y|$ components after the 15th wavenumber for the 2-D structure presented in the lower part of this Figure. E_{yi} stands for the inhomogeneous and E_{yh} for the homogeneous case.

In order to make comparison between the resolution of the dipole equatorial (both the transmitter and the receiver dipole are parallel to the strike direction, x) and the dipole axial array (when both dipoles are perpendicular to the strike, parallel to the axis y) the EM responses of the trench to the two arrays are presented in the same figure at the same frequency. Two conclusions can be made on the basis of the E_x, E_y modeling results presented in Figure 7, 8, 9, 10:

- the electric components at the frequency of f=1 Hz are more sensitive to the sea trench with this geometry than those at the frequency of f=0,1 Hz,
- amplitudes and phases of E_y over the trench to the dipole axial array has better resolution than the E_x responses calculated for the dipole equatorial array.

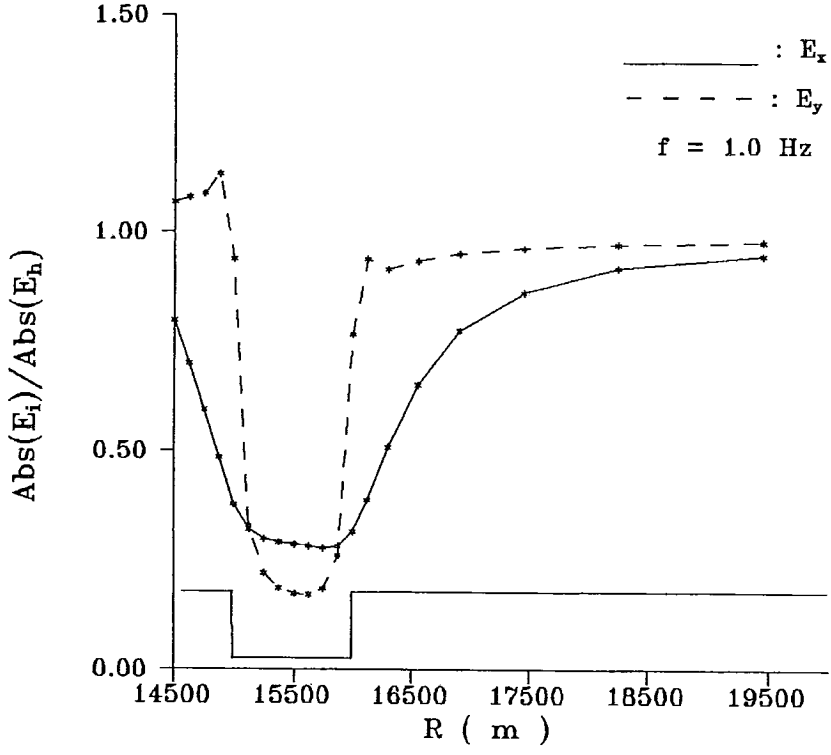

Fig. 7. Normalized amplitudes of the horizontal electric field components along the horizontal sea-bottom line over the 2-D seafloor trench at the frequency of f=1 Hz. E_x has been calculated for dipole equatorial, E_y for dipole axial array. The trench with 600 m depth and 1000 m width is situated at the range of 15 km $\leq R \leq$16 km as it is shown by the inset.

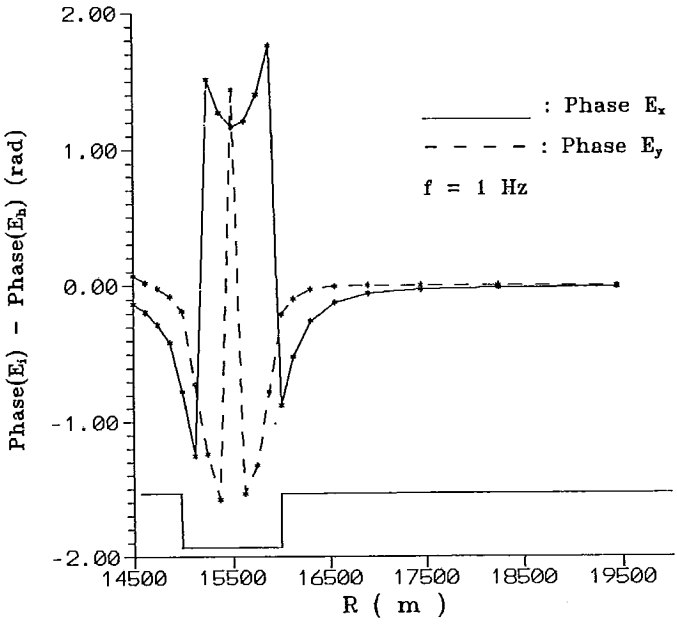

Fig. 8. Phase differences of the horizontal electric field components over the 2-D seafloor trench at the frequency of f=1 Hz. Otherwise see Figure 7.

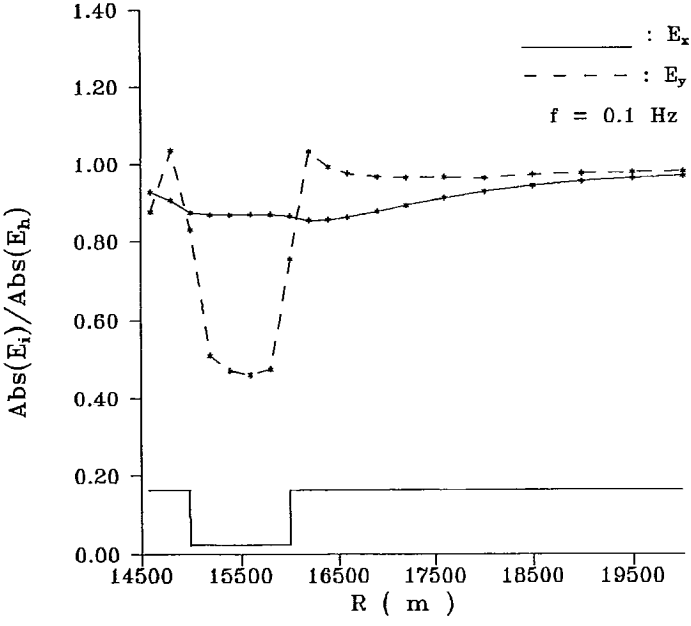

Fig. 9. Normalized amplitudes of the horizontal electric field components over the 2-D seafloor trench at the frequency of f=0,1 Hz.

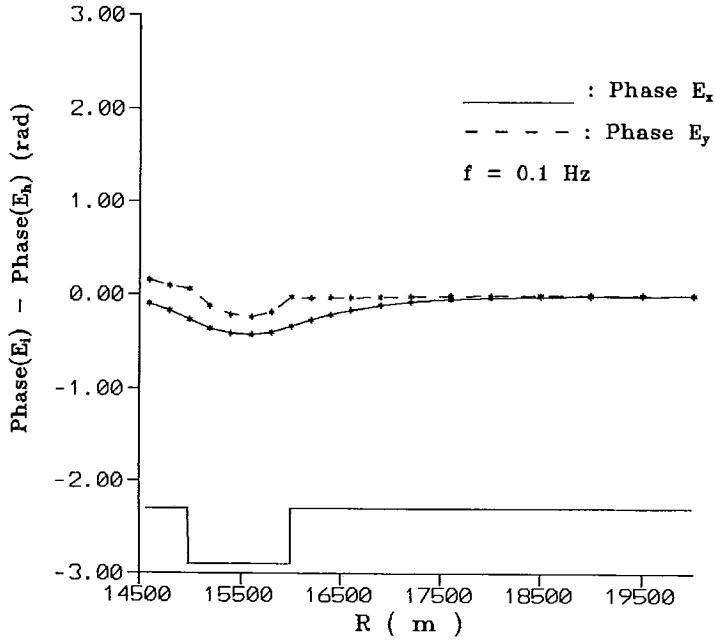

Fig. 10. Phase differences of horizontal electric field components over the 2-D seafloor trench at the frequency of f=0,1 Hz.

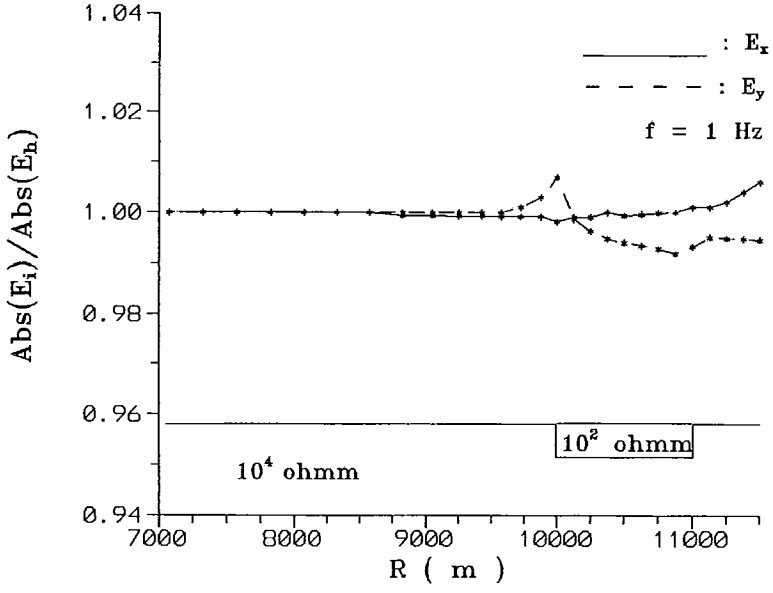

Fig. 11. Normalized amplitudes of the horizontal electric field components along the horizontal sea-bottom line over an alongated rectangular inhomogeneity at the frequency of f=1 Hz.

The latter statement is supported by E_x, E_y responses of the imbedded 2-D structure (its resistivity is ρ_3=100 Ωm, the elongated inhomogeneity has the same width (1000 m) and depth (600 m) as the sea trench has) in the Figure 11. Almost 1 % difference between the horizontal electric field components determined for the inhomogeneous and homogeneous model can be observed when the modeling was carried out in the dipole axial mode at f=1 Hz. This effect cannot be measured at this frequency, and in the other three situations the amplitude difference is even smaller.

The impedance responses are derived from the ratio of the horizontal electric field component to the horizontal magnetic field component perpendicular to it. The normalized impedances are presented in Figure 12, 13. Because of the electric charge accumulation along the vertical boundaries of the trench to dipole axial array, the impedance (Z_y=E_y/H_x) calculated from this array results in high lateral structural resolution as compared with that of the dipole equatorial array (Z_x=E_x/H_y). If the plane wave zone is approximated, the difference between the responses of HPOL mode and EPOL mode can be observed.

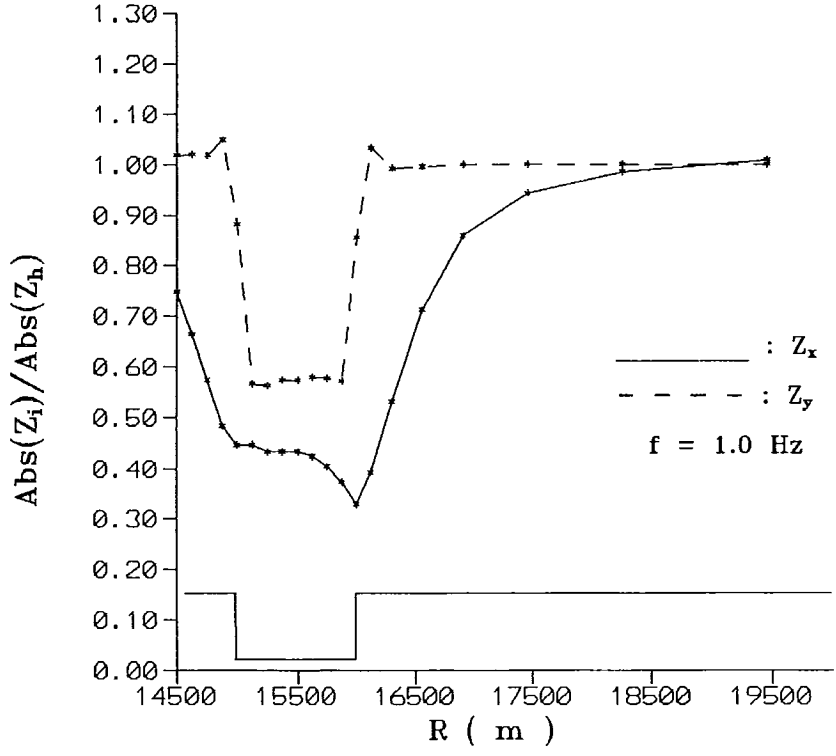

Fig. 12. Normalized absolute values of impedances for the two arrangements along the horizontal sea-bottom profile over the 2-D trench at the frequency of f=1 Hz. Z_x is derived from E_x/H_y (dipole equatorial array) and Z_y is from E_y/H_x (dipole axial array).

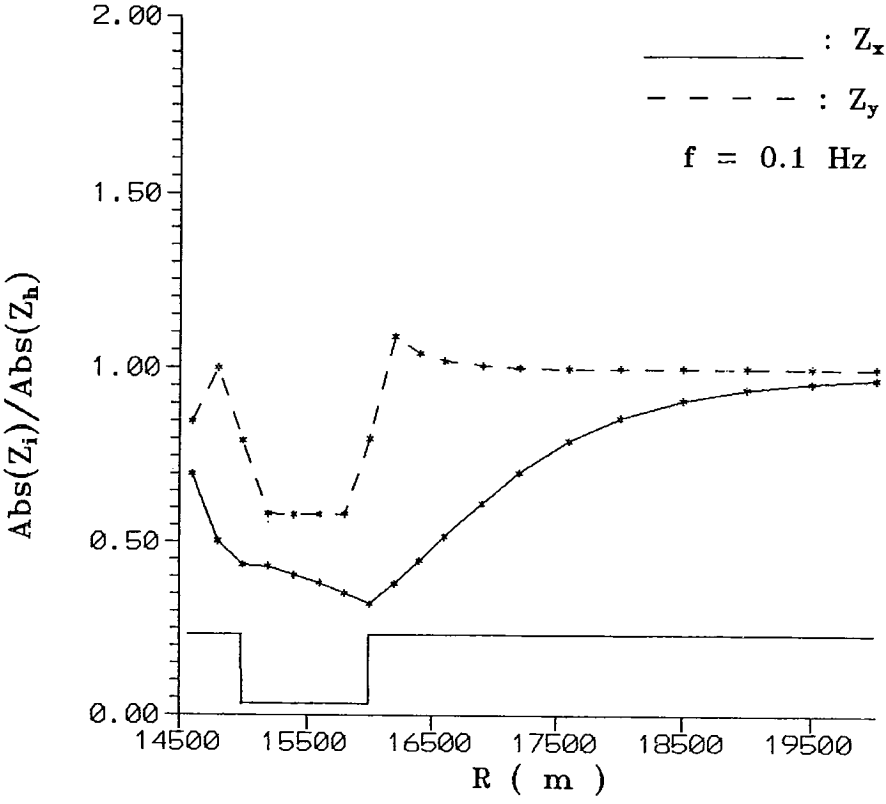

Fig. 13. The same as Figure 12 but at the frequency of f=0,1 Hz.

It is worth mentioning that H_z is strongly influenced by the topography of the seafloor. Assuming an along-strike electric source polarization we find that the H_z responses can be very sensitive indicators of sea trenches due to the magnetic fields induced by the along-strike current flow by the vertical walls. The relative amplitude response is presented in Figure 14.

Similarly to the vertical magnetic field component the vertical electric field component along the profile is affected by the conductivity inhomogeneties. Figure 15 shows what this effect is like at two frequencies to an electric source perpendicular to the geological strike. The relative E_z amplitude responses of the seafloor trench are presented.

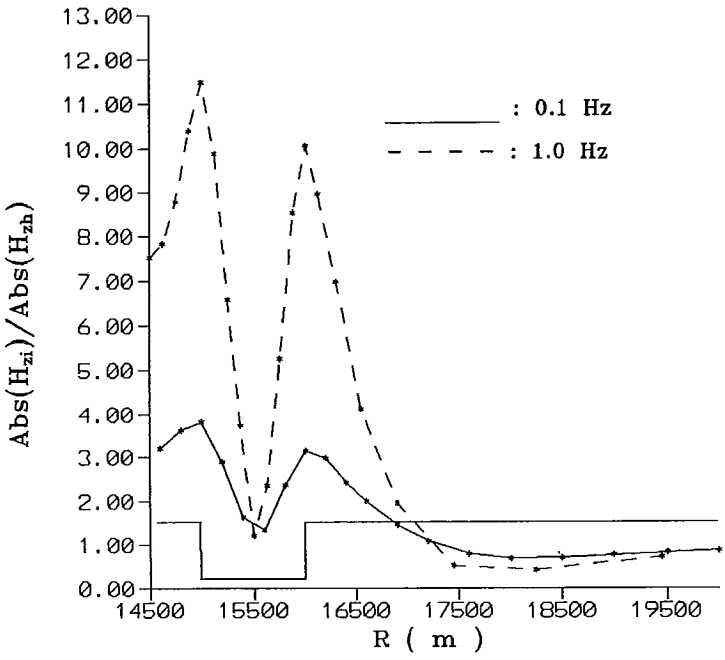

Fig. 14. Normalized $|H_z|$ components above the 2-D seafloor trench at frequencies of f=0,1 Hz and f=1 Hz.

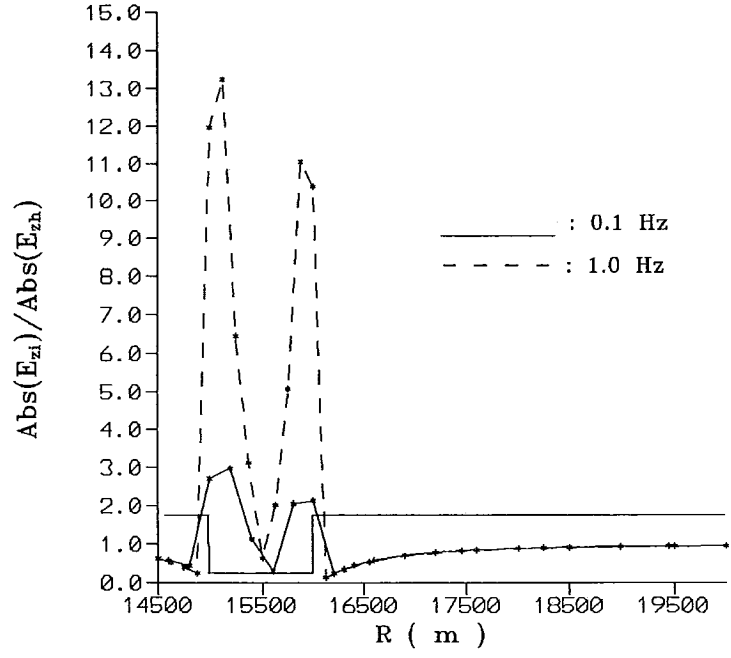

Fig. 15. Normalized $|E_z|$ components above the 2-D seafloor trench at two frequencies.

4. *Conclusions*

In order to make numerical modeling over a 2-D seafloor structure a finite-difference method was used to formulate the Fourier transform of Maxwell's equations in the along-strike wavenumber domain (k_x,y,z). In this way the original 3-D problem was transformed to a set of 2-D ones. The normalized EM field responses of a 2-D trench to a dipole equatorial and to a dipole axial array were presented along a horizontal in-line profile on the sea-bottom. This numerical modeling was not sufficient to investigate the effect of the 2-D seafloor topography on EM frequency sounding curves, but it has been established that these effects depend not only on the size of the inhomogeneity but also on the array and the frequency used. Comparisons between the two arrays were made at two frequencies of f=0,1 Hz and f=1 Hz. For the trench investigated it can be stated that the electric field responses determined for the in-line dipole axial array have better resolution than the electric field components of the in-line dipole equatorial array. The influence of the trench on EM field components depends on the frequency as well. Our results showed that the effect of the sea-bottom topography on all EM field components can be observed but in a different degree. H_z and E_z responses are particularly sensitive to these topographic changes and the use of the two source polarizations makes it possible to locate elongated sea-bottom trenches. The dipole axial array can be characterized by not only a better resolution but it is free from the effect of the trench at distances closer to the trech. If the task is the determination of the geoelectric parameters of the crust assumed to be 1-D, the in-line dipole axial array is preferred to the dipole equatorial one. In general, it can be stated that these topographical effects have to be taken into consideration to avoid the misinterpretation of frequency domain EM responses.

5. *References*

Anderson, W.L., 1979: Numerical Integration of Related Hankel Transforms of Orders 0 and 1 by Adaptive Digital Filtering. *Geophysics*, **44**, 1287-1305.

Chave, A.D. and C.S. Cox, 1982: Controlled Electromagnetic Sources for Measuring Electrical Conductivity Beneath the Oceans, 1. Forward Problem and Model Study. *Journal of Geophysical Research*, **87**, No. B7, 5327-5338.

Edwards, R.N. and A.D. Chave, 1986: A Transient Electric Dipole-Dipole Method for Mapping the Conductivity of the Sea Floor. *Geophysics*, **51**, 984-987.

Everett, M.E. and R.N. Edwards, 1993: Transient Marine Electromagnetics: the 2.5-D Forward Problem. *Geophys. J. Int.*, **113**, 545-561.

Pethő, G., 1987: Aspects of Finite Difference Modelling of the Electromagnetic Field of an Oscillating Electric Dipole. *Geophysical Transactions*, **33**, 113-122.

Pethő, G. and P. Kaikkonen, 1993: 2D Numerical Modelling of Frequency Sounding Using Horizontal Electric Dipole Sources. Paper presented at the 19th NOFTIG Meeting in Oulu, January 25-27, 1993.

Stoyer, C.H., 1974: Numerical Solutions of the Response of a Two-Dimensional Earth to an Oscillating Magnetic Dipole Source with Application to a Groundwater Field Study. Ph.D. Thesis, Pennsylvania State University.

Stoyer, C.H. and R.J. Greenfield, 1976: Numerical Solutions of the Response of a Two-Dimensional Earth to an Oscillating Magnetic Dipole Source. *Geophysics*, **41**, 519-530.

Szarka, L., 1993: 2-D Analog Model Measurement, Processing and Interpretation. Internal Report (in Hungarian), Geodetical and Geophysical Research Institute of the Hungarian Academy of Sciences, Sopron.

Takács, E., 1979: Finite Difference Solution of the EM Field due to a Magnetic Dipole Source over a 2-D Model. Internal Report (in Hungarian), University of Miskolc.

Unsworth, M.J., B.J. Travis and A.D. Chave, 1993: Electromagnetic Induction by a Finite Electric Dipole Source over a 2-D Earth. *Geophysics*, **58**, 198-214.